Advancing In-Space Precise Tracking: A Formation-Flying Picosatellites Mission

Centrella, Marianna; Speretta, S.; Uludag, M.S.; Stesina, Fabrizio

Publication date
2024

Published in
Proceedings of the 75th International Astronautical Conference

Citation (APA)
Centrella, M., Speretta, S., Uludag, M. S., & Stesina, F. (2024). Advancing In-Space Precise Tracking: A Formation-Flying Picosatellites Mission. In *Proceedings of the 75th International Astronautical Conference*

October 2024

Advancing In-Space Precise Tracking: A Formation-Flying Picosatellites Mission

Marianna Centrella[a*], Stefano Speretta[b], Mehmet Şevket Uludağ[c], Fabrizio Stesina[d]

[a] *Politecnico di Torino, Corso Duca degli Abruzzi 24, 10129 Torino, Italy,* marianna.centrella@studenti.polito.it
[b] *Delft University of Technology (TU Delft), Kluyverweg 1, 2629 HS Delft, The Netherlands,* S.Speretta@tudelft.nl
[c] *Delft University of Technology (TU Delft), Kluyverweg 1, 2629 HS Delft, The Netherlands,* M.S.Uludag@tudelft.nl
[d] *Politecnico di Torino, Corso Duca degli Abruzzi 24, 10129 Torino, Italy,* fabrizio.stesina@polito.it
[*] Corresponding Author

Abstract

In recent years, the trend towards satellite miniaturization has led to a considerable rise in picosatellite missions in Low Earth Orbit (LEO). Due to their size, identifying and tracking small objects poses significant challenges. While the detectability of individual picosatellites has been proven, the potential implications of clusters flying in formation remain unexplored. Therefore, the Delft University of Technology is starting a pioneering mission involving multiple picosatellites to improve Space Situational Awareness (SSA) by demonstrating the capabilities and limits of both in-space and ground-based tracking means.

This paper outlines a high-level mission analysis investigating the feasibility of this formation-flying mission: in the proposed model, the autonomy of each satellite is enhanced by integrating a Global Navigation Satellite System (GNSS) receiver, which enables independent orbital determination and facilitates the validation of satellite position data against other tracking systems. The mission concept involves deploying a cluster of two identical 3P PocketQubes, launched as a single spacecraft into a near-circular orbit. Following deployment, they will be separated using springs, considering factors such as relative velocity, direction, and angle to carefully study the release process. Additionally, their relative distance is controlled using differential drag, i.e. adjusting the satellite drag area by deploying solar panels at varying angles. Through the integrated use of STK and MATLAB, two mission control sequences are defined: the former, characterized by satellite propagation stopping conditions based solely on relative distance, and the latter, in which they are based on both relative distance and relative velocity. Their comparison reveals the latter as the most effective strategy: despite the challenge of controlling satellite distance during close passes (conjunctions), the optimal sequence prioritizes maximizing time in close proximity. This approach reduces the average relative velocity and minimizes the duration of the high drag configuration, resulting in a significant extension of the mission lifetime. The simulations, along with a power budget, support the definition of both mission and GNSS receiver payload requirements. Finally, a suitable candidate is selected from among miniaturized GNSS space receivers and tested through multiple hardware-in-the-loop simulations, using a GNSS signal simulator. These simulations aim at verifying the accuracy of receiver positioning measurements and assessing power consumption.

The results of this paper represent the cornerstone of a disruptive mission, providing insights into the future development of satellite control optimization strategies to minimize collision risk. Furthermore, the remarkable payload test results, while reliable, underscore the need to improve testing systems to reduce position errors and achieve higher tracking accuracy for LEO picosatellites equipped with GNSS receivers.

Keywords: Mission Analysis, Picosatellites Tracking, PocketQubes, Formation-flying, System Engineering, GNSS Receivers

1. Introduction

In recent years, small satellite missions have become increasingly popular due to the availability of affordable launch opportunities and cutting-edge technologies that allowed scaling down component dimensions. Furthermore, since small satellites generally have lower complexity and fewer payloads compared to larger satellites, they can be manufactured at higher production rates [1]. Today, small satellites are widely used for various applications, such as Earth observation, technology demonstration, and educational missions. Small satellites are commonly divided into several categories [2], including picosatellites, which have a mass ranging from 0.1 kg to 1 kg. A picosatellite platform that has sparked the interest of the space community since its first appearance in 2009 [3] is the PocketQube (PQ). One-eighth smaller than a CubeSat in terms of volume, the PocketQube unit (1P) is 50 mm x 50 mm x 50 mm in size [4] and can be combined with other units to create larger form factors, such as 3P or 6P.

As of May 2024, 83 PQs have been launched [5], including 22 in the past year alone, reflecting a rapid increase in picosatellite missions, with most of them still operational. Overall, the number of active satellites in Low Earth Orbit (LEO) has been steadily increasing, rising from 1000 in 2014 to approximately 6700 in 2023 [6] [7]. This exponential growth is expected to continue in the coming years.
As orbital traffic in LEO rises, so does the hazard of collision between objects, which could generate a significant amount of space debris that may remain in orbit for years, posing a threat to operational satellites. Mitigating this risk is a key objective of the Space Situational Awareness (SSA), a core component of the EU Space Programme [8], and is accomplished through a process known as Space Surveillance and Tracking (SST). The risk of creating orbital debris is further increased if the satellites are as small as picosatellites, which are among the most challenging to identify and track, particularly during the initial phases of rideshare missions. While individual PocketQubes have already been successfully tracked, the implications of deploying a formation-flying cluster have yet to be studied.
Within this framework, the Delft University of Technology is building a space mission with multiple picosatellites flying in formation, primarily to demonstrate the current status of tracking performance by in-space (e.g. Global Navigation Satellite System (GNSS) Receiver) and ground-based means used for SSA purposes. This paper deals with the high-level mission analysis and system design, aims to confirm its feasibility, and lays the foundation for a mission never explored before.

The main objectives, the mission concept, and the research goals of this work will be presented in Section 2. In the upcoming paragraphs, the mission analysis and the methodology used will be introduced first (Section 3), and then, the simulations results will be shown and discussed (Section 4), leading to the establishment of high-level mission requirements. The preliminary design of the GNSS receiver payload will be presented in Section 5, including a power analysis and a detailed overview of the hardware-in-the-loop (HIL) simulations performed. Ultimately, conclusions and insights for future work will be drawn in Section 6.

2. A Picosatellite Mission

This section provides an overview of the mission, presenting its objectives first, its high-level implementation, and ultimately its scientific goals.

2.1 Mission Objectives

A novel mission involving a cluster of picosatellites is currently being developed at the Delft University of Technology, as part of the Delfi Space Program, a development line focused on very small satellites [9]. The program started in 2004, with three general mission objectives: education, technology demonstration, and small satellite bus development. Over the years, the Delfi Team has already launched three satellites, including two 3U CubeSats in 2008 and 2013, and a 3P PocketQube in 2022. The latest satellite, Delfi-PQ (shown in Figure 1), has paved the way for a significant trend toward miniaturization, and its legacy is now driving the development of a new mission.

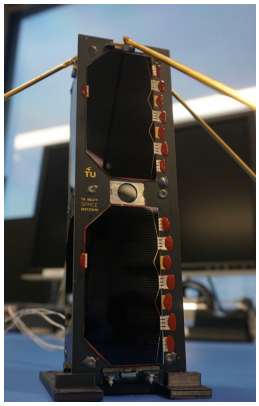

Fig. 1: Delfi-PQ

This mission comprises multiple picosatellites, which have limited capabilities in terms of Precise Orbit Determination (POD), as well as extremely small radar and optical cross-sections, making them challenging to detect [10]. The uncertainty in their positions increases the risk of collisions [11], which must be mitigated. Therefore, the mission aims to evaluate the tracking capabilities and limits of different sensors used for SSA [10], which can be based on ground, such as space surveillance radars, laser tracking systems, optical sensors, and radio transmissions, or used in space. Several systems will be integrated in the satellites to enhance their trackability, including Light-Emitting Diodes (LED)s, which increase their visibility, and GNSS receivers, that provide satellite position data for validation against tracking systems. This also enables independent orbital determination, particularly important during a conjunction - an event in which two satellites are estimated to pass near each other [12] - to validate conjunction prediction algorithms.
In summary, the mission goals would be [10]:

- Demonstrate in-space precise tracking of multiple pico- and femto-satellites down to accuracies better than what currently achievable with publicly available Two Line Elements (TLEs).
- Demonstrate ground tracking (by means of radar, optical and laser tracking) of femto-satellites and assess

the achievable orbital elements accuracies.

- Test in-space identification of space objects using laser and optical instruments.
- Provide independent position measurements for two objects involved in a conjunction.

2.2 Mission Concept

The mission architecture features a twin satellite formation consisting of two identical 3P PocketQubes: each one will carry a range of payloads, including LEDs and a miniaturized GNSS receiver. The satellite core bus will include the Electrical Power System (EPS), Command and Data Handling System (CDH), and Communication System (COMM), based on the Delfi-PQ design. Furthermore, the satellites will not have thrusters for attitude control and will therefore experience random rotations along the three axes. One method for controlling their position will involve adjusting their drag area, for example, by extending a solar panel and varying its deployment angle over time.
The satellites will be launched as a single spacecraft into a near-circular orbit of approximately 500 km, a common altitude for most commercial launches, no earlier than 2025. Once in orbit, they will be separated upon command by springs into two identical and independent satellites, which will then fly in formation. The mission lifetime must ensure at least 6 months of operational life before natural re-entry.

2.3 Research Goals

Within this context, the research goals of this work can be summarised as follows:

- **Study of satellite in-flight separation and control via differential drag.** The analyses must assess plausible values for relative separation velocities to optimize the time the satellites spend in close proximity. Moreover, to ensure the satellite safety during close passes, or conjunctions, the safest directions of separation and detachment angles should be evaluated. To maintain satellite formation, changes in drag area can be achieved by deploying solar panels at varying angles, whose effects on the satellite lifetime need to be analysed.
- **High-level requirements elicitation.** At the beginning of this work, several requirements were already defined by the Delfi Team and used as input in the simulations conducted. However, the ultimate goal of the mission analysis is to establish new technical requirements to guide the design and development of the mission. The initial requirements, as well as those derived from the mission analysis, are summarized in Table 8, along with their Identifiers (ID).
- **Payload design: the GNSS receiver.** Since the GNSS receiver is an essential payload of this mission, the aim is to find a space-capable receiver that uses an acceptable amount of power within the limits of the total power available for payloads. Once a suitable receiver is selected, its accuracy in positioning measurement should be tested and its power consumption should be verified.

3. Mission Analysis

The high-level mission analysis is performed to study mission feasibility and measure performance. For this purpose, several scenarios are defined in Systems Tool Kit (STK), enabling to model complex systems to provide a realistic 3D simulation environment for digital mission engineering [13]. In particular, the STK Astrogator module is used to propagate the satellites by defining a Mission Control Sequence (MCS), that is a series of actions to be performed by each satellite. This section initially outlines the common characteristics of the scenarios, followed by an in-depth explanation of the MCSs.

3.1 Scenario Configuration in STK

In a new STK scenario, the first element to be defined is the start time, which is set to 15 July 2025 at 12:00:00.000 Coordinated Universal Time (UTC), taking into account that the mission timeline schedules a launch no earlier than 2025. On the other hand, the stop time constrains the analysis period to one or four months, depending on the simulation. Subsequently, two satellite objects, named FirstQube and SecondQube (see Figure 2), are included in the scenario. The spacecraft properties are edited considering the characteristics of the PocketQubes to be analysed, which will be introduced in the next subsection. In all simulations, the relative motion of the satellites is described through the Radial / In-Track / Cross-Track (RIC) reference frame, a local coordinate system centered on FirstQube, against which all relative distances and velocities are calculated.

3.2 Mission Control Sequences

Each satellite control sequence is a collection of segments, customized to the input requirements. The following provides an overview of the segments used within the Astrogator sequences and their features.

- **Initial State (IS).** To specify the "Initial State" of the satellites, first the orbital elements are set according to Table 1.

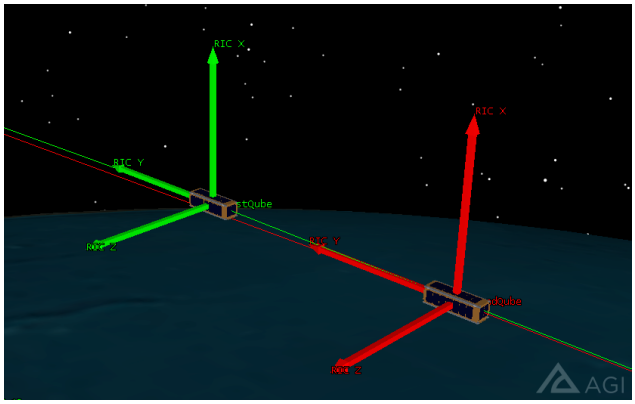

Fig. 2: FirstQube (green RIC axes) and SecondQube (red RIC axes) in the initial phases of a scenario. The 3U CubeSat model, visible in the figure, is chosen only for visualization, as a PocketQube model is not available in STK.

Table 1: Keplerian Elements.

a $[km]$	***e***	***i*** [°]	**RAAN** [°]	ω [°]
6878.14	1.0E-4	97.5	0	0

Thus, the two PocketQubes are placed into a 500 km circular, Sun-synchronous orbit.
To complete the definition of the "Initial State", various spacecraft parameters are set. The value of the Dry Mass, equal to 0.545 kg, was provided by the Delfi Team, as well as the values of the Drag Coefficient (C_d) and drag area, obtained by fitting the Delfi-PQ orbital decay. The drag model is kept spherical as per default setting, while the Solar Radiation Pressure (SRP) and the Radiation Pressure (RP) (albedo and thermal) are also set as shown in Table 2.

Table 2: S/C Parameters.

Drag		SRP		RP	
$\mathbf{C_d}$	**Area** $[m^2]$	$\mathbf{C_r}$	**Area** $[m^2]$	$\mathbf{C_k}$	**Area** $[m^2]$
2.2	0.02	1	0.02	1	0.02

- **Propagate (P).** The Earth High-Precision Orbit Propagator (HPOP) is used to propagate the spacecrafts, considering the following force models: a gravitational field model (EGM2008), third-body gravity (Moon and Sun, both considered as point mass), solar radiation pressure, and atmospheric drag (Jacchia-Roberts Atmospheric Density Model). The latter exerts a perturbing force on a satellite orbiting Earth, causing the acceleration represented in STK by the following equation [14]:

$$a_D = -\, C_D \, \frac{A_D}{M} \, \frac{\rho V^2}{2} \qquad [1]$$

where:

  - C_D is the drag coefficient;
  - A_D is the satellite cross-sectional area along the velocity vector. It is also known as drag area;
  - M is the satellite mass;
  - ρ is the atmosphere density;
  - V is the satellite speed relative to the atmosphere.

The minus sign indicates that the drag force acts in the direction opposite to the velocity vector V. Equation 1 also introduces a key parameter, $\frac{M}{C_D A_D}$, known as the ballistic coefficient. The higher the ballistic coefficient, the longer the satellite lifetime. This is because atmospheric drag decreases the orbit kinetic [15], gradually lowering the satellite altitude. Variations in drag area result in different ballistic coefficients for two satellites flying in formation, leading to differential drag [16].
The "Propagate" segments are defined by both the orbit propagator and the Stopping Conditions (SC), which determine where, when, or how to initiate actions or terminate propagation [17]. The SC used in this work are as follows:

  - Duration: propagation stops after a specified time duration.
  - Epoch: propagation stops on a specified time and time.
  - Range: propagation stops when the range between the two satellites reaches a specified value.

- **Maneuver (M).** This segment allows one to specify the features of a finite or impulsive burn to be performed by a satellite object. In the context of this work, an impulsive maneuver is modeled using Cartesian or spherical coordinates relative to the satellite's RIC axes. This approach simulates the velocity imparted by the spring forces upon satellite separation, which occurs on 15 July 2025 at 12:00:05.000 UTC in all simulations. This implies a separation occurring with a latitude of 0.143 deg, i.e. at the equator.

- **Update (U).** Through the "Update" segment, it is possible to change the spacecraft parameters, previously set in the initial state, as needed. Basically, it serves to update the drag area value in most analyses.

Two different sequences are built to study the effects of using differential drag as a method to keep the formation flying, and thus involve changes in drag area. The MCSs differ as the satellite motion is controlled differently: Sequence-1 (S1) bases the stopping conditions only on relative distance, while in Sequence-2 (S2) the stopping conditions rely on both relative distance and relative velocity. The two sequences, divided in multiple stages, are now introduced. To run them in different steps, allowing one to iterate on different parameters and to act on both satellites in one simulation, STK is integrated with MATLAB via the STK Programming Interface.

3.2.1 Sequence-1: Relative Distance

1° Step: The trajectory of SecondQube begins by setting the initial state and performing a preliminary propagation for a few seconds. Subsequently, the separation caused by the release spring force is simulated, and the satellite is then propagated until the stop time of the scenario.

2° Step: The trajectory of FirstQube is run. After defining the initial state and simulating the spring separation, the satellite propagates away from the other until it reaches a specific maximum distance. Its drag area is now instantaneously increased, and the satellite propagates approaching SecondQube until the point of minimum distance (on which no constraints have been set). At this point, the drag area is reduced and the satellite propagates again to the distance marked as maximum, and then to the end of the scenario.

3° Step: Before starting the third run, the final time of the last propagation of FirstQube until the maximum distance, $T^{\mathbf{fin}}_{\mathbf{P_{4a}}}$, is extrapolated and set equal to the initial time of P_{2b}, the first "Propagate" segment of SecondQube after separation (see Table 3). This means that once the simulation has started, and after separation, SecondQube propagates freely until this specified time. Then, the drag area is increased and decreased, as in the 2° Step, and the satellite propagates until the end-of-scenario epoch.

Table 3: Sequence-1. All the SC after satellite separation are based on the relative distance, i.e. range.

FirstQube	SecondQube
	IS_b: Initial State
	P_{1b}: Until Duration SC
	M_b: Spring Force
	P_b: Until Epoch SC
IS_a: Initial State	
P_{1a}: Until Duration SC	
M_a: Spring Force	
P_{2a}: Until Max Range SC	
U_{1a}: Increase Drag Area	
P_{3a}: Until Min Range SC	
U_{2a}: Decrease Drag Area	
P_{4a}: Until Max Range SC	
P_{5a}: Until Epoch SC	
	$T^{\mathbf{in}}_{\mathbf{P_{2b}}} = T^{\mathbf{fin}}_{\mathbf{P_{4a}}}$
	IS_b: Initial State
	P_{1b}: Until Duration SC
	M_b: Spring Force
	P_{2b}: Until Max Range SC
	U_{1b}: Increase Drag Area
	P_{3b}: Until Min Range SC
	U_{2b}: Decrease Drag Area
	P_{4b}: Until Max Range SC
	P_{5b}: Until Epoch SC

3.2.2 Sequence-2: Relative Distance - Relative Velocity

1° Step: The trajectory of SecondQube is propagated for few seconds and, afterward, separation due to the release spring force is performed, and the satellite propagates until the end of the scenario.

2° Step: The trajectory of FirstQube is run. After defining the initial state and simulating the spring separation, the satellite drifts away from the other with a constant positive average relative velocity, until it reaches a specific maximum distance, when the drag area is instantaneously increased. At this point, in this case, FirstQube does not directly propagate approaching SecondQube until the point of minimum distance, but it propagates in a high-drag configuration only for a limited period of

Table 4: Sequence-2. The SC after satellite separation are based on both the relative distance and the relative velocity.

FirstQube	SecondQube
	IS_b: Initial State
	P_{1b}: Until Duration SC
	M_b: Spring Force
	P_b: Until Epoch SC
IS_a: Initial State	
P_{1a}: Until Duration SC	
M_a: Spring Force	
P_{2a}: Until Max Range SC	
U_{1a}: Increase Drag Area	
$T^{\mathbf{fin}}_{\mathbf{P_{3a}}} = T^{\mathbf{avg.rel.vel}}$	
P_{3a}: Until Epoch SC	
U_{2a}: Decrease Drag Area	
P_{4a}: Until Min Range SC	
P_{5a}: Until Max Range SC	
P_{6a}: Until Epoch SC	
	$T^{\mathbf{in}}_{\mathbf{P_{2b}}} = T^{\mathbf{fin}}_{\mathbf{P_{5a}}}$
	IS_b: Initial State
	P_{1b}: Until Duration SC
	M_b: Spring Force
	P_{2b}: Until Max Range SC
	U_{1b}: Increase Drag Area
	$T^{\mathbf{fin}}_{\mathbf{P_{3b}}} = T^{\mathbf{avg.rel.vel}}$
	P_{3b}: Until Epoch SC
	U_{2b}: Decrease Drag Area
	U_{4b}: Until Min Range SC
	P_{5b}: Until Max Range SC
	P_{6b}: Until Epoch SC

time, that is, until its average relative approaching velocity is exactly opposite to the average velocity with which they are moving away. At that time, the drag area is decreased. FirstQube then propagates approaching SecondQube reaching first the point of minimum distance, then the point of maximum relative distance, and finally the end of the scenario. To ensure the calculation of the time point $T^{\mathbf{avg.rel.vel}}$, at which the escaping relative velocity reaches a value opposite to the approaching one, this step is in turn executed through two successive runs of the FirstQube trajectory.

3° Step: Before starting the last run, it is extrapolated the final time of the last propagation of FirstQube until the maximum distance, that is $T^{\mathbf{fin}}_{\mathbf{P_{5a}}}$, and set equal to the initial time of P_{2b}, the first "Propagate" segment of SecondQube after separation (see Table 4). Therefore, once the simulation has started and after the separation, SecondQube propagates freely until this specified time. From this point on, the SecondQube trajectory is the same as that of FirstQube, with a brief increase in drag area, before further propagation phases towards the end-of-scenario epoch.

The relative motion between the satellites (see Figures 3 and 4) can be explained by the fact that both the impulsive maneuver associated with the spring force release and the increase in drag area simulate a "retrograde burn". In these sequences, the retrograde thrust occurs in the opposite direction with respect to the "target" and the direction of motion, when the "chaser" is behind the target (FirstQube and SecondQube will exchange these roles). Therefore, the chaser first drifts away from the target for a brief period and then approaches because it loses altitude and begins to accelerate [18]. A conjunction is reached and the chaser continues in its motion with higher velocity, until new actions are taken, such as decreasing the drag area of the chaser or increasing the drag area of the target, which will then become the new chaser. From an orbital dynamics point of view, the higher acceleration of the chaser is due to the fact that with a retrograde thrust the chaser will be in an elliptical orbit approaching perigee and, therefore, accelerating. This orbit has a smaller period than the original one, causing the chaser to arrive at its starting point somewhat earlier [18]. This orbital mechanics effect can be explained physically also through the conservation

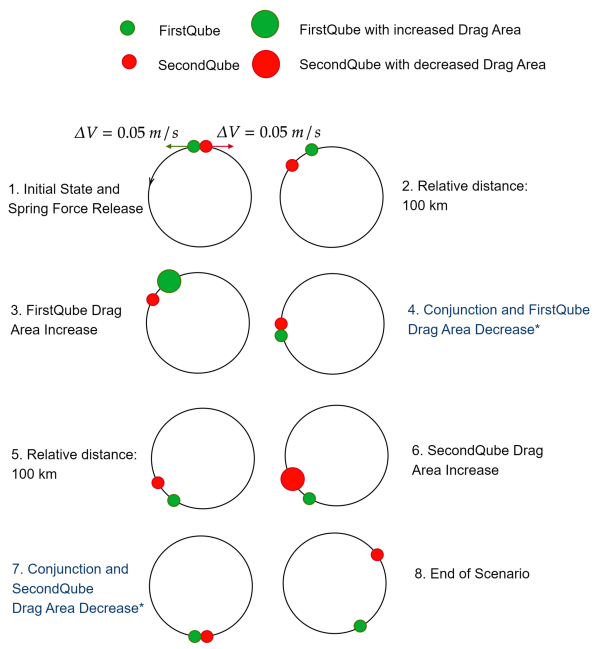

Fig. 3: This graphical representation (not to scale) is independent of time and actual orbits, and is intended only to illustrate the relative positions of satellites resulting from changes in drag area during the implementation of Sequence-1. *The Drag Area Decrease occurs when the satellites reach the point of minimum relative distance.

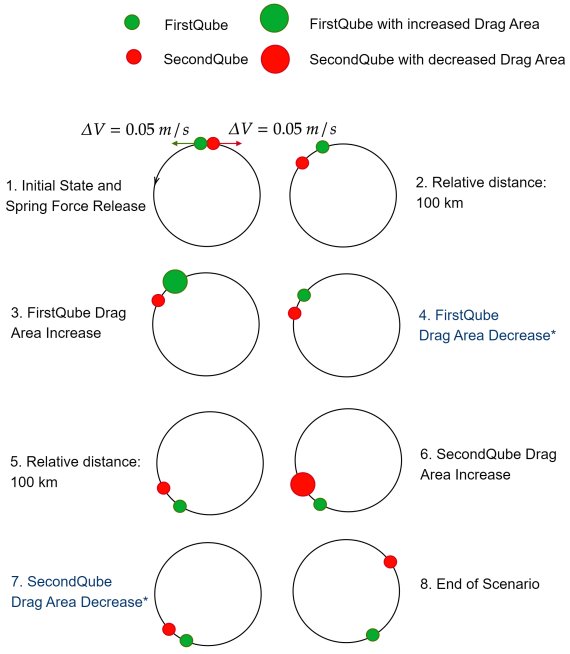

Fig. 4: This graphical representation (not to scale) is independent of time and actual orbits, and is intended only to illustrate the relative positions of satellites resulting from changes in drag area during the implementation of Sequence-2. *The Drag Area Decrease occurs when the average relative approaching velocity is exactly opposite to the average velocity with which they are moving away.

of the total mechanical energy, which implies that if the satellite gains altitude it has to slow down, while if it loses altitude it has to speed up [19].

4. Simulation Results

Once the two sequences have been implemented, they are used to study the scenarios at multiple stages, evaluating the initial satellite release process with respect to direction, velocity, and angle. The sequences are then compared to each other to investigate the consequences of drag variations under different stopping conditions and their impact on mission lifetime.

4.1 Drag Area Control: Preliminary analysis results

The first preliminary analysis involves determining the ideal direction of separation, regardless of the magnitude of the relative velocity at the beginning of the scenario, also referred to as the separation velocity. It is discovered that the In-Track direction, that is, along the velocity vector, is the safest, as it widely reduces the risk of collision compared to the Cross-Track or Radial direction.
Another initial analysis focuses on the separation velocity, which is set to 10 cm/s, taking into account the magnitude of the forces released by commercially available springs [20, 21]. To simulate the separation process, a "Maneuver" segment is defined in STK, allowing both satellites to perform an impulsive maneuver: a change of velocity ΔV is set to +5 cm/s along the thrust axis for FirstQube and equal to -5 cm/s for SecondQube, on the same thrust axis. With this choice, the satellites would have a low initial relative velocity and would orbit for several days within a relative distance of 100 km, established as the limit for Close Proximity Operations (CPO). Such operations encompass various activities, including conjunctions, that the satellites perform within a relatively close area, ranging from a few meters to tens of kilometers [22], depending on mission characteristics.
The outcomes of these preliminary simulations are used as input for the subsequent ones.

4.2 Drag Area Control: Sequence-1

In this analysis, Sequence-1, with stopping conditions based only on relative distance, is implemented. In particular, the stopping condition concerning the satellite maximum range is set to 100 km (as highlighted by the line drawn in Figure 5) for CPO purposes. On the other hand, the minimum range is set to 3 km to ensure algorithm convergence. After defining the other segments, the "Update" one is also configured, which is especially useful for adjusting the drag area. The simulation is carried out with 2x, 3x and 4x drag area increment factors.

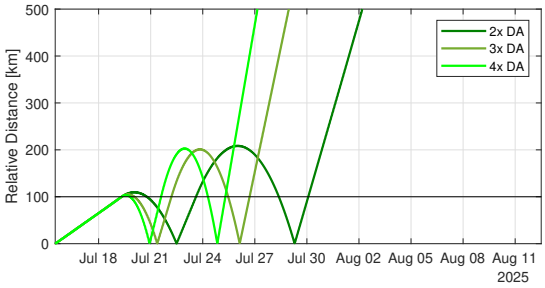

Fig. 5: Relative Distance as a function of an increasing Drag Area (DA).

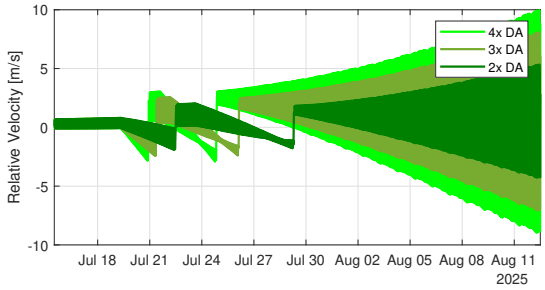

Fig. 6: Relative Velocity as a function of an increasing Drag Area (DA).

With Sequence-1, the drag area is increased and decreased only once per satellite. Therefore, once SecondQube gains 100 km relative to FirstQube, the satellites move away freely until the end of the scenario. The entire process results in the overshoots depicted in Figure 5, indicating that the satellites move beyond 100 km away before a new conjunction occurs. Ideally, these overshoots should be avoided to maximise the time spent in close proximity. That being the goal, it is decided to continue the simulations by doubling the drag area, since Figure 5 clearly shows that a smaller increase in drag area results in the satellites orbiting in close proximity for a longer time. Additionally, Figure 6 demonstrates that, with a 2x drag area increment, the relative velocity oscillates within a lower range over time, causing the satellites to take longer to drift apart.

4.3 Drag Area Control: Sequence-2 + S1-S2 Comparison

Controlling overshoots is not achievable with Sequence-1, as stopping conditions placed both on relative distance and relative velocity are needed. Indeed, Sequence-2 allows the satellites in the neighborhoods of conjunctions to maintain an average relative velocity that matches the initial average relative velocity established immediately after their separation. As a result, the satellites move more slowly and their orbiting time within

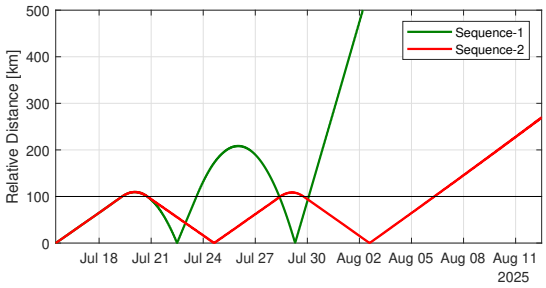

Fig. 7: Relative Distance calculated with the two control strategies.

the CPO spatial range increases, reducing overshoots. To analyse the advantages and drawbacks of S2 relative to S1, the figures discussed below present a comparison between the two.

Considering the mixed control strategy over distance and velocity in S2, the overshoot magnitude is limited to 110 km (see Figure 7) and does not increase with the number of close passes. In addition, the time between two conjunctions increases and the satellites spend more time in close proximity. These two features, which are also verified by incrementing the number of close passes between the satellites, are advantageous because they could theoretically reduce the frequency of commands needed from ground operators. However, Sequence-2 lacks control over the minimum distance between satellites during conjunctions, which can fall significantly below the collision risk threshold of 1000 meters. Therefore, it may be necessary to introduce new stopping conditions when the satellites approach one another. The implications of such changes will have to be explored.

Figure 8 shows that the velocity fluctuations are greatly reduced with S2, causing the satellites to move slower, which is confirmed to be one of the major assets of this sequence. In fact, from Figure 9 stands out that the numerical value of average relative velocity at the first close pass decreases in absolute value from 1 m/s in S1 to 30 cm/s in S2, thus matching the relative velocity achieved after the satellite initial detachment. The average relative velocity is calculated in MATLAB through a moving average filter.

During the time frame when conjunctions occur (as pointed out in Figure 9), the relative velocity seems to switch almost instantaneously from a negative to a positive value. In reality, the velocity remains constant and the apparent sign change is simply a result of how relative velocity accounts for the direction of motion. Nevertheless, this change in sign, due to the chosen notation, allows for displaying whether the satellites are moving away (indicated by a positive relative velocity) or approaching each other (indicated by a negative relative velocity).

Comparing the two implemented sequences reveals another advantage of the mixed control strategy: it leads to a significant reduction in the time each satellite spends in a high-drag configuration, which is when its drag area is wider. By considering an analysis period with only one drag area variation (increase and decrease) per satellite, the average duration of the high-drag configuration is calculated: 4.38 days over a period of 13.77 days for S1, while 1.31 days over a period of 14.28 days for S2. Thus, already in the short term, the duration requiring a higher drag area is decreased by approximately 3 days. Spending less time in high-drag conditions results in reduced braking and slower altitude loss, which would extend the satellite lifespan and allow for more months of in-orbit operations. Indeed, over an entire analysis period, the average value of drag area, i.e. the cross-sectional area values (0.0264 m^2 for S1, 0.0219 m^2 for S2), are used to estimate the satellite lifetime through simulations run with DRAMA. Sequence-1 guarantees a lifetime of 6 months, whereas, using Sequence-2, a lifetime of 7.5 months is foreseen. Therefore, 1.5 months are gained, resulting in a margin over the minimum mission duration of 6 months set by the initial requirement (see Table 8).

In light of these reasons, it is clear that an optimal con-

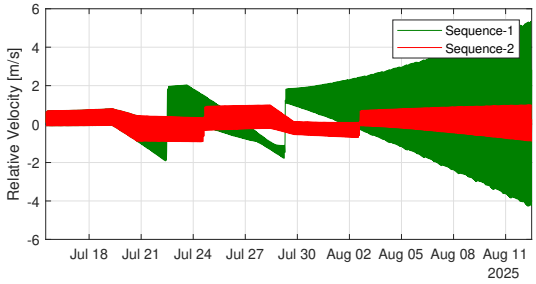

Fig. 8: Relative Velocity calculated with the two control strategies.

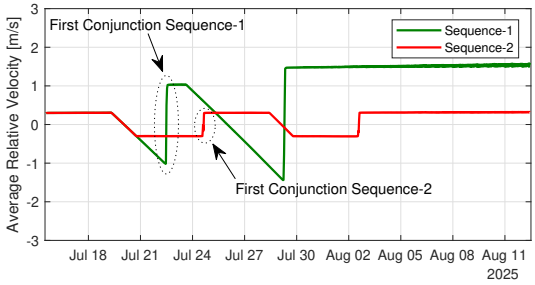

Fig. 9: Average Relative Velocity calculated with the two control strategies.

trol strategy would take into account stopping conditions based on both relative distance and relative velocity.

4.4 Limiting Angle of Satellite Separation

Until this point, all simulations have assumed satellite separation aligned with the In-Track direction, as this has been proven the most reliable way to avoid collisions. However, considering the potential challenges of stabilizing satellite attitude and the possibility of satellite spin, it is important to explore whether other separation directions might also be safe. To prevent collisions, it is crucial to ensure that the satellites maintain a distance of at least 1000 m during their first and most critical conjunction. Therefore, to determine if there is a limiting angle beyond which a collision is inevitable, two different simulations are carried out:

- (A): Fixing a given Elevation angle, iteration over 14 Azimuth angles, spacing from the Radial / In-Track (XY) plane towards the Radial / Cross-Track (XZ) plane (see Figure 10).
- (B): Fixing a given Azimuth angle, iteration over 14 Elevation angles, spacing from the In-Track / Cross-Track (YZ) plane towards the Radial / Cross-Track (XZ) plane.

For these simulations, Sequence-1 is used, keeping the same orbital dynamics as described in Section 3. Opting to use Sequence-2 would made no difference, as the focus is on what happens during the first conjunction after a single orbit, which lasts about 94 minutes. The reference frame used is a customized RIC local system centered on the satellite's center of mass. FirstQube is used in these analyses.
The azimuth and elevation angles are shown in Figure 10. The vector of 14 angles, which can refer either to azimuth or elevation, is defined as follows:

[angles] = [0, 10, 15, 20, 30, 40, 45, 50, 60, 70, 75, 80, 85, 88]°;

These angles, together with the magnitude, constitute the tern of spherical coordinates (Az, El, Mag) that characterizes the impulsive maneuver in STK. In all simulations, the magnitude is set at ±5 cm/s to reflect the previously assumed relative separation velocity of 10 cm/s. For the sake of clarity, the azimuth and elevation angles are calculated differently by STK, and the conversion factors between one system to the other are provided as follows:

$$\mathrm{Az}_{\mathrm{custom}} = \mathrm{El}_{\mathrm{stk}}$$
$$\mathrm{El}_{\mathrm{custom}} = 90 - \mathrm{Az}_{\mathrm{stk}}$$

However, the simulations input parameters in azimuth and elevation are taken with respect to the customized reference system.

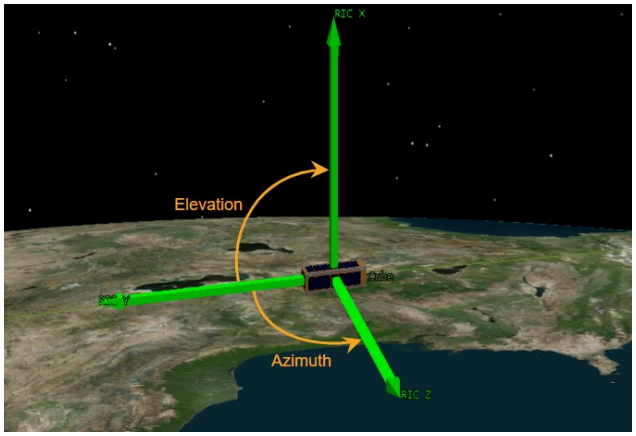

Fig. 10: Radial / In-Track / Cross-Track (XYZ) reference system centered on FirstQube, in STK. Azimuth (Az) and Elevation (El) angles are shown. The direction of motion coincides with the positive direction of the Y axis.

Table 5: Azimuth - Elevation angles for Simulation (A).

FirstQube	**SecondQube**
El = x	El = 180° + x
Az = [angles]	Az = -[angles]

Table 6: Azimuth - Elevation angles for Simulation (B).

FirstQube	**SecondQube**
Az = x	Az = - x
El = [angles]	El = 180° + [angles]

By fixing an elevation angle and iterating over the 14 azimuth angles, simulation (A) is repeated for N=17 values to find the azimuth limiting angle (*) beyond which the satellite would collide. On the other hand, the elevation limiting angle (*) is found by running simulation (B) for N=16 values, with a fixed azimuth angle, iterating over 14 elevation angles. These critical angles are collected in Table 7 and shown in Figure 11.
By connecting these points between them and to the satellite's center of mass and projecting them on the Radial / In-Track plane, it is possible to define a spatial region where separating the satellites can be considered safe. Moreover, the effects of a separation in other symmetric directions should give similar results in terms of limiting angles. Therefore, by mirroring the curve displayed in Figure 11 across different planes of symmetry, a cone is defined (see Figure 12). Its vertex coincides with the satellite's center of mass, while its half-aperture angle is calculated consid-

Table 7: Azimuth and Elevation Limiting Angles.

Simulation (A)		Simulation (B)	
El [°]	**Az* [°]**	**Az [°]**	**El* [°]**
0	52.7	0	53.4
5	52.6	5	53.2
10	52.2	10	52.7
13	51.8	13	52.3
15	51.4	15	51.9
20	50.3	20	50.7
25	48.6	25	49.0
30	46.3	30	46.5
35	43.1	35	43.3
40	38.8	40	38.7
45	32.4	45	32.1
50	22.0	50	21.0
51	19.0	51	17.4
52	15.1	52	12.3
52.5	12.3	52.5	7.10
53	8.40	53	does not exist
54	does not exist	54	does not exist

ering the limiting angle relative to the direction of motion. To this end, the projection of the (Az, El) coordinates (as detailed in Table 7) along this direction is computed. The angle relative to the direction of motion is then calculated using the following formula:

$$\theta = arcsin(\sqrt{sin(Az)^2 + sin(El)^2}) \qquad [2]$$

For the coordinates of simulation (A), it is found that:

$$\theta_{min} = 52.7° \quad \theta_{max} = 63.7°$$

while for simulation (B):

$$\theta_{min} = 53.4° \quad \theta_{max} = 63.8°$$

The global minimum defines the half-aperture angle of the cone, thus equal to:

$$\theta = 52.7°$$

4.5 High-Level Mission Requirements

Table 8 shows the initial mission and system requirements, set by the Delfi Team, as well as collects all the new requirements that are derived from the mission analysis carried out throughout this research. These requirements range from ID MIS-100 to ID MIS-130.

5. GNSS Receiver High-Level Design

To select a suitable GNSS receiver for this mission, a power budget is first conducted to determine how much

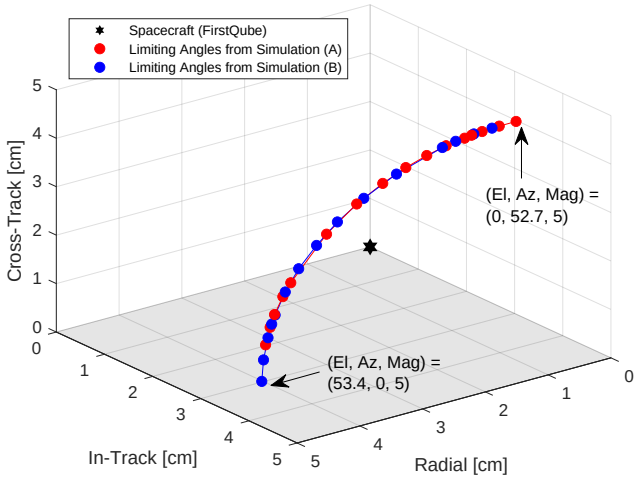

Fig. 11: Limiting Angles from Simulation (A) and (B).

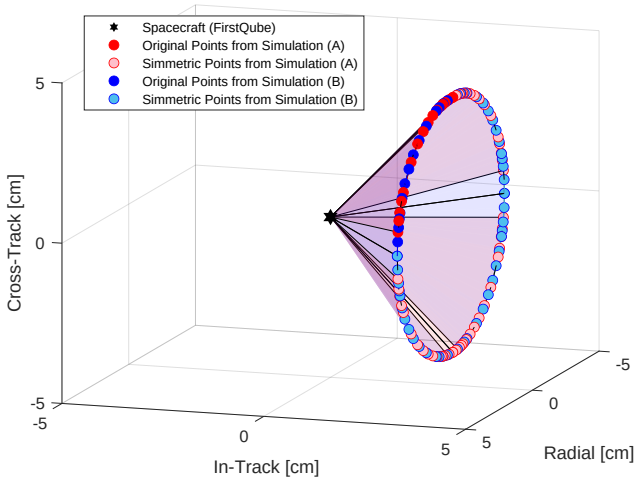

Fig. 12: The set of points that defines the region of space beyond which satellite separation leads to a relative distance greater than 1000 m at the first close pass.

power is available to allocate to all payloads. The outcomes of the power analysis, along with the mission architecture, contribute to establishing payload system requirements, which will constrain the receiver selection process.

5.1 Power Budget

The power budget is an analysis used to assess the total available power and the amount required by all spacecraft elements to ensure proper operation. In this context, it includes the three core-bus subsystems: EPS, CDH, COMM. The power estimate depends on the mission phase and, in this case, is performed for the nominal mode (see Table 9), which is when the subsystems require maximum Orbit Average Power (OAP).
The OAP is computed by taking into account several fac-

Table 8: Mission and System Requirements.

ID	Requirement
MIS-010	Two 3P PocketQubes shall at least be developed.
MIS-020	The mission shall target a launch in 2025.
MIS-030	The critical mission lifetime shall be equal to at least 6 months.
MIS-040	The satellites shall be released in an orbital range of 475-525 km.
MIS-050	The separation of the satellites shall occur upon command.
MIS-060	The characteristics for the lowest orbit possible shall be limited by a minimum mission lifetime equal to the critical mission lifetime.
MIS-070	The orbit inclination range shall be 95-105 deg.
MIS-080	The mission cost shall be less than 300k Euro, including launch and operations.
MIS-090	The mission shall be compliant with ESA's Space Debris Mitigation Guidelines.
MIS-100	The initial relative separation velocity shall be equal to 10 cm/s.
MIS-110	The drag area shall be increased and decreased by a factor of two.
MIS-120	The drag area variations shall be managed by a control strategy that takes into account at least relative distance and relative velocity.
MIS-130	The satellite separation shall occur within the region of space bounded by a cone (Fig. 12) centered on the center of mass of one of the satellites and with a maximum half-aperture angle of 52.7°.
SAT-010	Each satellite must be equipped with a core segment with space heritage.
SAT-020	The core segment of each satellite shall be composed of the following subsystems: EPS, CDH, COMM, STR (Structural System), TCS (Thermal Control System).
SAT-030	The space segment mass shall be less than 1.5 kg.
SAT-040	All systems of the each satellite shall survive the launch environment.
SAT-050	All systems of each satellite shall be able to cope with the space environment.

tors: the Best Engineering Estimate (BEE), which is the estimated resource value, based on available data from Delfi-PQ; the contingency, a margin expressed as a percentage of the BEE, added to it to account for uncertainties and risks (for these subsystems, it is set to 1%, as the values of the BEE are derived from measurements of Delfi-PQ final flight hardware); the duty cycles, which refer to the percentage of time a subsystem is actively operating at its nominal power level relative to the total time, and in this case are set to the maximum allowed percentage.
Table 9 shows that the total consumed power turns out to be equal to 207 mW, a rather low value compared to the total available power. The latter is calculated with a simulation run through STK Solar Panel Tool. Specifically, a PocketQube 3P with 8 AzurSpace solar cells, each with an area of 30.18 cm^2 and an efficiency of 28.1%, is considered as a reference, and a conversion is implemented to perform the power analysis directly with the CubeSat model present in STK. Moreover, a satellite random spin around two rotational axes is assumed, with an average rotation velocity equal to ω = 1.67 rev/s, again derived from Delfi-PQ available data. The simulation indicates that the total available power is equal to 1127 mW, leading to a power surplus of 920 mW. This amount of power is to be used not only by the GNSS receiver but also by other payloads, including the LEDs. Based on the power estimates of the other payloads, the GNSS receiver power consumption shall be less than 0.5 W. In addition, assuming a margin relative to the 3P PocketQube boards dimensions of 42 mm x 42 mm, it is determined that the GNSS receiver size shall be less than 40 mm x 30 mm.

Table 9: Power Budget for Nominal Mode.

Subsystem	Mode	BEE + Contingency [mW]	Duty Cycle	OAP [mW]
EPS	On	45.45	100.00%	45
CDH	On	30.30	100.00%	30
COMM	Receive	105.62	95.00%	100
	Transceive	375.34	8.30%	31
		Total Consumed Power [mW]:		207
		Total Available Power [mW]:		1127
		Budget surplus/deficit [mW]:		920

5.2 GNSS Receiver Selection

Given these requirements, a suitable receiver for this mission is sought, with priority given to selecting a space-capable receiver that does not yet have flight heritage, for technology demonstration purposes. After extensive market research, the choice is made in favor of the SkyTraq S1316F8-G13, a single-frequency receiver used for vehi-

Table 10: SkyTraq GNSS Receiver features.

Model Supplier	Antenna	Power [W]	Mass [gr]	Size [mm]
S1216F8-GI3 SkyTraq	1	0.40	2	12 x 16

cle navigation, asset tracking, and time synchronization applications [23]. Some features of this receiver are shown in Table 10, derived from [24].

5.3 HIL GNSS Signal Simulation

The aforementioned SkyTraq receiver is used to perform GNSS HIL signal simulations, aimed at testing the accuracy of the receiver in returning satellite position measurements. To this end, a CoCom-free firmware is applied on this receiver, meaning that its functionality is not limited if the device is in LEO orbit, thus beyond a certain altitude, or moving faster than a specific speed. Testing the receiver in a simulated environment will also be useful in assessing its power consumption.

5.3.1 Setup and Process

The simulation setup includes:

- An open-source software, Software-Defined GPS Signal Simulator (GPS-SDR-SIM) [25].
- A computer owned by the Delft University of Technology, with GNU Radio open-source software installed.
- A USRP Software Defined Radio (SDR).
- A signal manual attenuator (see Figure 13a).
- A DC-block.
- The SkyTraq S1316F8-G13 receiver, installed on a board (see Figure 13b).

The GNSS signal emulation is based on the open-source software GPS-SDR-SIM, thus only GPS signals can be simulated. Specifically, in a dynamic simulation, when the user specifies a trajectory arc, i.e. "User Motion File" (UMF), and a GPS satellite constellation (e.g. RINEX navigation file), the GPS-SDR-SIM generates GPS baseband signal data streams, which include simulated pseudorange and Doppler information for the GPS satellites in view. The data streams are converted to radio-frequency signals through the SDR platform, and transmitted to the receiver for playback. Therefore, during the simulations, the SDR platform transmitter port is connected to the board of the GNSS receiver through the attenuator and the DC block, while the receiver board is, in turn, connected to the computer via a USB cable. The data streams arriving at the receiver will have to be logged in a "LOG" file, saved, and post-processed.

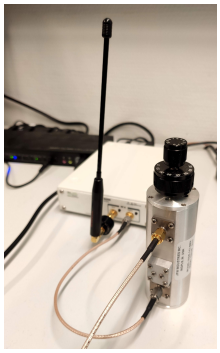

(a)

(b)

Fig. 13: URSP Radio and Attenuator (a) and SkyTraq S1316F8-G13 GNSS Receiver installed on a board (b).

In the following, a specific trajectory arc, called "Increase", is considered as a reference, and refers to a 5-minute arc when one of the satellites doubles its drag area in the STK scenario (longer arcs produce data volumes too large for the system in use). More in detail, the simulation process involves several steps to be followed:

1. Download the Rinex navigation file and provide the "Increase" trajectory arc, or UMF, as input to GPS-SDR-SIM software by specifying the following command line on the GNU Radio Command Prompt:
   - gps-sdr-sim -e Rinex\brdc2650.23n -u usermotion.csv

   where the UMF ("usermotion.csv") is given in ECEF x,y,z format and shown in Table 11. It should be noted that regardless of the start time of the trajectory arc in the scenario, the start point of this simulation coincides with the initial instant of the RINEX file ("brdc2650.23n", updated to 22 September 2023). As a result, a binary file ("gpssim.bin") is created and saved.

Table 11: UMF for the "Increase" Trajectory Arc.

Relative Time	x^{UMF}_{ECEF} [km]	y^{UMF}_{ECEF} [km]	z^{UMF}_{ECEF} [km]
0	-3632	3899	4333
0.1	-3632	3899	4332
0.2	-3632	3900	4331
...	...	...	...
300	-3997	5052	2379

2. Create an empty LOG file ("log.csv") where to save the logged data.
3. Start to read the data from the GNSS receiver, using a dedicated Python file, here called "serial_reader_mc.py", which forces a receiver cold start

each time the script is launched. Run the following command line on the Anaconda Command Prompt:

- python serial_reader_mc.py -l log.csv

4. Playback the binary file, transmitting it to the GNSS receiver through the SDR, the attenuator and the DC-block. To this end, run the following command line on the GNU Radio Command Prompt:

   - python gps-sdr-sim-uhd.py -t gpssim.bin -s 2600000 -x 30

   where "gps-sdr-sim-uhd.py" is a Python file present in the GPS-SDR-SIM software suite, "2600000" is the sampling rate to be used and "30" is the radio-frequency gain to be used.

5. Wait for the 3D Fix (acquisition of latitude, longitude and altitude) to be acquired and then lost, then check the LOG file with the recorded data, an example of which is shown in Table 12. The GNSS 3D Fix provides position data in LAT, LON, ALT coordinates, with latitude and longitude measured in degrees with directional indicators (North, South, East, West) in reference to the Earth's equator and prime meridian. Altitude is measured in meters above the WGS84 reference ellipsoid. It is worth noting that the time elapsed between the cold start and the acquisition of the 3D Fix is the cold start Time To First Fix (TTFF).

Table 12: LOG File for the "Increase" Trajectory Arc.

UTC Time	UTC Date	LAT	LON	ALT	Fix Type
11:59:45	28/06/2006	0.0N	0.0E	0 km	No
...	...	...	...	...	...
00:00:30	22/09/2023	0.0N	0.0E	0 km	No
00:00:31	22/09/2023	36.2N	132.1E	497 km	No
00:00:32	22/09/2023	36.1N	132.1E	497 km	No

5.3.2 GNSS Receiver Position Accuracy

One approach to determine the GNSS receiver position accuracy is to compare the LOG file, with data derived as output from the receiver, with the UMF, which includes the input trajectories data streams. For this purpose, it is required to:

- Transform the LAT, LON, ALT coordinates of the LOG file into ECEF coordinates of the UMF file;
- Correlate the UTC time of the LOG file to the relative time of the UMF.

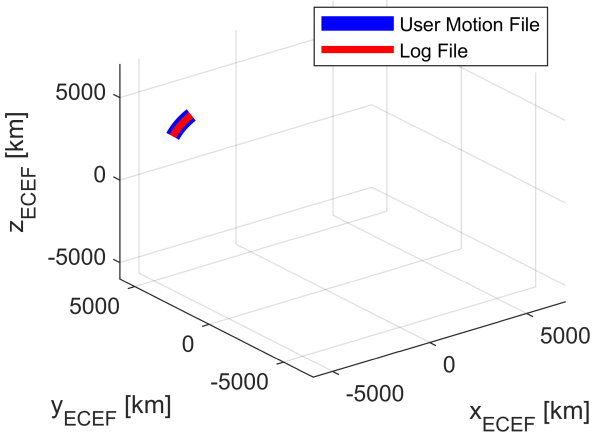

Fig. 14: 3D Graph of the "Increase" Trajectory Arc: Comparison between UMF and LOG file.

These aspects are addressed in a MATLAB script, from which a 3D graph is derived (see Figure 14), showing the apparent complete overlap, on a kilometer scale, of the UMF and the LOG file.
Therefore, to more precisely evaluate the position error, it is calculated as the difference between the actual input position and the simulated position along each of the three axes. These differences are determined using the following formulas and are shown in Figure 15.

$$\begin{aligned} \Delta x &= x_{ECEF}^{UMF} - x_{ECEF}^{LOG} \\ \Delta y &= y_{ECEF}^{UMF} - y_{ECEF}^{LOG} \\ \Delta z &= z_{ECEF}^{UMF} - z_{ECEF}^{LOG} \end{aligned} \quad [3]$$

The position error ranges from a few meters to several tens of meters in each direction. Thus, the Root Mean Square Error (RMSE) is computed using Equation 4, and for the "Increase" trajectory arc, is found to be:

$$rmse = \sqrt{\Delta x^2 + \Delta y^2 + \Delta z^2} = 21.4\ m \quad [4]$$

The same GNSS HIL simulation is also run for three other trajectory arcs, and the following results are obtained:

Table 13: RMSE for various Trajectory Arcs.

Trajectory Arc	Description	Arc Duration [s]	RMSE [m]
Initial State	At the beginning of the scenario	300	50.1
Conjunction	At the first satellite conjunction	300	26.6
Stop Scenario	On the last day of the scenario	300	25.7

According to the SkyTraq receiver datasheet [23], the receiver is expected to have an accuracy of approximately

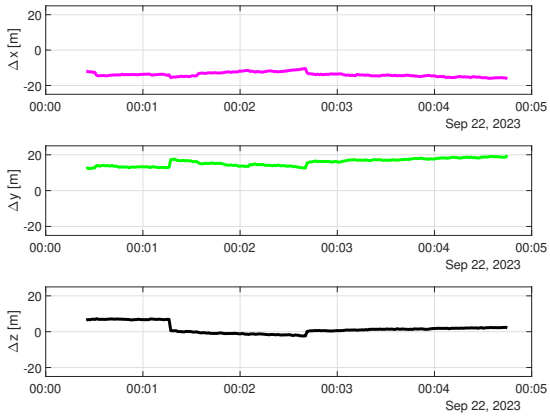

Fig. 15: Position Error for the "Increase" Trajectory Arc.

2.5 m Circular Error Probable (CEP). However, the observed accuracies are higher, with RMSE ranging from about 20 m to 50 m. Nevertheless, the measurements are deemed reliable, considering the limitations of the system:

- The GPS-SDR-SIM software does not compensate for ionospheric refraction, which is a major source of error for a single-frequency GNSS receiver. On the other hand, the receiver in use applies ionospheric correction, resulting in a position error. To enhance performance, the receiver's option for correcting ionospheric refraction should be disabled.
- For commercial-off-the-shelf receivers, the on-board navigation solution providing position, velocity, and time information also involve a periodic error due to the receiver real-time navigation algorithm. Indeed, it does not account for Coriolis acceleration, an apparent force that, however, becomes non-negligible at the high velocities at which the satellite moves [26].

Additionally, the "Initial State" RMSE of 50.8 m, which is rather high compared to the others, could be explained by the fact that this is the only trajectory arc in which the satellites cross the equatorial region. In [26], by fitting the orbital models to on-board navigation solution, it is found that the RAAN estimate is affected by an error due to a systematic rotation of the orbital plane, which leads to a periodic error with maximum magnitude at the equator, where it is of the order of tens of meters. This results to an error in the estimation of orbital parameters, and thus in the accuracy of orbit determination.

5.3.3 GNSS Receiver Power Consumption

The power consumption of the SkyTraq S1216F8-GI3 receiver is obtained by connecting the receiver to a power supply during data transmission, and it turns out to be 110 mA at 3.3 V. To determine the total power consumption of the GNSS receiver payload during operations, the other components of the final board housing it within the satellite must also be considered: a low-noise amplifier, with consumption of 10 mA at 3.3 V, and a processor/SD card, with consumption of 15 mA at 3.3 V. Therefore, the total consumption of the GNSS receiver payload in nominal mode is equal to 0.445 W. As a consequence, the nominal-mode power budget is updated by considering a 30% contingency due to the conceptual nature of the data, and by setting the duty cycle at 80% to account for the receiver not being constantly active during an orbit. With these changes, the OAP required by the GNSS receiver is 0.463 W, complying with the initially defined requirement (see Section 5.1). In addition, around 0.457 W of power remains available to accommodate other payloads.

6. Conclusions and Future Work

Throughout this paper, the high-level mission analysis of a future Delft University of Technology picosatellite mission is performed. The mission concept includes two formation-flying 3P PocketQube, separated in orbit through separation springs and controlled by means of differential drag. Ensuring a minimum of 6 months of lifetime, the simulations confirm the mission feasibility. This is reflected in the establishment of high-level mission requirements that address the separation angle and velocity, the variation of the drag area, and the satellite control strategy. Each PocketQube is required to carry a GNSS receiver as a payload for precise positioning measurements, which is essential to fulfilling several mission objectives. To test the selected receiver, four HIL GNSS signal simulations are conducted, achieving positioning accuracy in the range of tens of meters, and maintaining power consumption within the total available power for payloads.
Future mission analysis should include proper investigation of satellite separation mechanisms to ensure precise separation velocities, as well as exploring methods to modify the drag area. Furthermore, the satellite control strategy should be optimized to mitigate collision risks and extend mission lifetime. In the context of GNSS signal simulations, addressing and overcoming system limitations will be a key point to minimize position error.

Acknowledgements

This publication is based on the Master's Thesis project of the first author: "Mission and System Design of a Formation-Flying Picosatellites Cluster: A Technology Demonstration Mission for Space Situational Awareness Improvement". She conducted this study as a visiting student at the Space Systems Engineering Department of

the Faculty of Aerospace Engineering, Delft University of Technology. She is grateful to Stefano Speretta, Mehmet Şevket Uludağ, Eberhard Gill, and Fabrizio Stesina for their support of her research and for the hospitality provided.

References

[1] S.M. Spremo, A.R. Crocker, and T.L. Panontin, "Small Spacecraft Overview," 2019.

[2] Small Spacecraft Systems Virtual Institute, "State-of-the-Art Small Spacecraft Technology," 2021.

[3] B. Twiggs, "Making it Small." Cal Poly Developers' Workshop, California State Polytechnic University, San Luis Obispo, CA, 2009.

[4] Alba Orbital, TU Delft, and Gauss Srl, "The PocketQube Standard." Issue 1, 2018, https://www.albaorbital.com/pocketqube-standard, (accessed 04.08.23).

[5] E. Kulu, "PocketQubes." 2023, https://www.nanosats.eu/, (accessed 25.08.24).

[6] L. Grego, "Update of UCS Satellite Database." 2023, https://blog.ucsusa.org/lgrego/update-of-ucs-satellite-database-2/, (accessed 27.08.23).

[7] Union of Concerned Scientists, "UCS Satellite Database." 2024, https://www.ucsusa.org/resources/satellite-database, (accessed 25.08.24).

[8] European Union Agency for Space Programme, "Space Situational Awareness." 2024, https://www.euspa.europa.eu/european-space/space-situational-awareness, (accessed 25.08.24).

[9] T. Delft, "Delfi Program." 2024, https://www.tudelft.nl/lr/delfi-space/delfi-program, (accessed 25.08.24).

[10] S. Speretta, M.S. Uludag, A. Menicucci, and I. Ferrario, "Space Surveillance Network Capabilities Evaluation Mission," *Proceedings of 2nd NEO and Debris Detection Conference*, vol. 2, 2023.

[11] United States Government Accountability Office, "Large Constellations of Satellites: Mitigating Environmental and Other Effects," 2002.

[12] M. Scott Balch, R. Martin, and S. Ferson, "Satellite conjunction analysis and the false confidence theorem," *Proc. R. Soc. A*, vol. 475:20180565, 2019.

[13] Ansys Inc., "Ansys STK." 2023, https://www.ansys.com/products/missions/ansys-stk, (accessed 05.08.23).

[14] Ansys Inc., "Technical Notes for HPOP." 2023, https://help.agi.com/stk/, (accessed 06.10.23).

[15] B.D. Tapley, B.E. Shutz, and G.H. Born , *Statistical Orbit Determination*. Elsevier, 2004.

[16] B.S. Kumar, A. Ng, K. Yoshihara, and A. D. Ruiter, "Differential Drag as a Means of Spacecraft Formation Control," *IEEE Transactions on Aerospace and Electronic Systems*, 2011.

[17] Ansys Inc., "Stopping Conditions." 2023, https://help.agi.com/stk/, (accessed 07.08.23).

[18] Mission Operations Directorate, *Rendezvous and Proximity Operations Handbook Part 2*. National Aeronautics and Space Administration, USA, 1988.

[19] R.R. Bate, D.D. Mueller, J.E. White, and W.W. Saylor, *Fundamentals of Astrodynamics - Second Edition*. Dover, New York, 2021.

[20] R. Hiler, "Design of a CubeSat Separation Mechanism," *Honors Theses*, vol. 2794, 2017.

[21] R.L. Burton and V.L. Coverston et Al., "Initial development of the cubesail/ultrasail spacecraft," *Joint Army Navy NASA Air Force (JANNAF) Spacecraft Propulsion Subcommittee Meeting*, 2010.

[22] Y.Z. Luo, Z.J. Sun, and J. Zhang, "Proximity scenario design for geostationary rendezvous with collocated satellite avoidance," *Acta Astronautica*, vol. 154, pp. 153–168, 2019.

[23] SkyTraq Technology Inc., "S1216F8-GI3." 2023, https://www.skytraq.com.tw/homesite/home-product, (accessed 10.10.23).

[24] E. Gill, J. Morton, P. Axelrad, D.M. Akos, M. Centrella, and S. Speretta, "Overview of Space-Capable Global Navigation Satellite Systems Receivers: Heritage, Status and the Trend towards Miniaturization," *Sensors*, 2023, 23, 7648.

[25] T. Ebinuma, "GPS-SDR-SIM." 2023, https://github.com/osqzss/gps-sdr-sim, (accessed 10.10.23).

[26] L. Müller, L. Chen, G. Möller, M. Rothacher, B. Soja, and L. Lopez, "Real-time navigation solutions of low-cost off-the-shelf GNSS receivers on board the Astrocast constellation satellites," *Advances in Space Research*, 2023.